



Parametric Optimization on Single Point Incremental Forming of Aluminum Alloy AA 2219-O using Response Surface Methodology

Umair Khalil¹ · Muhammad Haris Aziz² · Summyia Qamar¹ · Khurram Munir³

Received: 7 October 2020 / Accepted: 25 September 2022 / Published online: 21 October 2022
© King Fahd University of Petroleum & Minerals 2022

Abstract

Single Point Incremental Forming (SPIF) is an emerging sheet metal forming process which has been used in the prototype production of complex geometries. The geometric inaccuracies and quality of formed parts are the major obstructions in commercialization of SPIF process. The aim of presented work is to study this hindrance using experimental and numerical investigation on Aluminum Alloy 2210-O. Parametric optimization is done using Response Surface Methodology (RSM) for quality factor (surface roughness) and geometric accuracy (Maximum wall angle) while minimizing thickness reduction and forming time. For this purpose, three experimental setups were designed in this study, using tool types and tool paths. During investigation, the interaction and main effects of process parameters, viz. feed rate, spindle speed, and step increment are evaluated on surface roughness (R_a), maximum wall angle (α_{max}), % thickness reduction (% TR), and forming time (T) using ANOVA method. Results showed that among all the parameters of SPIF process, step increment is the most significant parameter for both forming paths using ball end and flat end tool. The comparative analysis of this study suggested that the ball end tool using the bidirectional path was better than the other setups. Furthermore, the results revealed that the ball end tool using a spiral path was better in desirability achievement (73%) as compared to the flat end tool using a spiral path (71.2%). The findings of this study are beneficial in paving a path for optimization of the SPIF process for an industrial-scale production of Al alloy AA 2219-O with desired characteristics.

Keywords Single point incremental sheet forming · Aluminum Alloy AA2219-O · Response surface methodology · Geometric accuracy · Optimization

1 Introduction

Single point incremental sheet forming (SPIF) is a novel and cost-effective sheet metal forming process in which no additional dies are required. The elimination of pre-fabricated dies in this manufacturing process reduces the cost per workpiece and increases productivity [1]. The whole SPIF process can be performed on CNC machines using simple forming tools for an incremental deformation of the sheets to produce a variety of parts. One of the benefits of using SPIF

is the reduction in the lead time consumed in tool development and investment cost. Different studies investigated the SPIF process to explore various characteristics of the process such as forming limit curves [2] _ENREF_13 discussed forming limit curve to explain the difference between fracture limit and necking limit, forming force and time [3] discussed relationship of cracks with forming force and time, friction effect [4] discussed the effect of friction stir assisted SPIF on formability, and microstructure and deformation behavior [5] studied microstructure and deformation behavior of aluminum alloy. Moreover, this process can be performed on a wide range of materials. Various studies have reported the process-ability of SPIF process using different materials such as Zhang et al. [6] worked on magnesium alloy (AZ31) to study the effect of lubricating methods, Hussain et al. [7] worked on commercially pure titanium (CP Ti), and Franzen et al. [8] worked on polyvinyl chloride (PVC) sheets. SPIF processes have been extensively investigated in

✉ Muhammad Haris Aziz
harisquireshi444@gmail.com

¹ Industrial Engineering Department, University of Engineering and Technology, Taxila 47080, Pakistan

² Mechanical Engineering Department, College of Engineering and Technology, University of Sargodha, Sargodha, Pakistan

³ School of Engineering, RMIT University Bundoora East Campus, Mill Park, Victoria 3083, Australia



recent years as they offer several advantages over the conventional forming processes including higher formability, shorter lead times, lower initial costs and greater process flexibility [9–11].

Moreover, extensive research has been carried out to investigate the effect of various forming factors on forming properties. Prashant et al. [12] studied the effect of hemispherical *forming tool* on Al alloy 3003-H14. The study reported best formability, reduced noise, and low wear with hemispherical tool. Ziran et al. [13] suggested that the flat end tool exhibits better formability, while Silva et al. [14] supported a freely rotating ball tool for decreasing friction between the forming sheet and tool. Likewise, *step increment* has also a significant effect on the quality of a formed path. Malwad, Nandedkar [15] studied deformation mechanism analysis of SPIF process on AA 8011. They concluded that the surface roughness decreases by decreasing the step increment. Jagtap et al. [16] also supported the results in their study of surface roughness and thickness analysis using Al-1050 using a hemispherical tool. However, Rattanachan, Chungchoo [17] reported an inverse relationship between step increment and surface roughness on DIN 1.003 steel, i.e., surface roughness increases by increasing the step increment. Cavaler et al. [18] and Bagudanch et al. [19] reported similar results for AISI 304L Stainless steel and thermoplastic material, respectively. Formability is also dependent on the *feed rate*. Davidson et al. [20] found that feed rate is the most significant factor which effects the surface roughness of AA-6061 and it increases with increase in the feed rate, while the experimental study of Mulay et al. [21]_ENREF_43 using AA5052-H32 showed that surface roughness decreases with an increase in the feed rate. Thus, the contradictory results imply that the effect of process parameters depends on the material being formed. Furthermore, springback phenomenon in Incremental Sheet Forming (ISF) process is characterized by the *forming path*. Kopac, Kampus [22] examined that for better results, the forming should be done from the inner to the outer boundary of the sheet. Cui, Gao [23] studied a multi-stage forming strategy with small increments in wall angle and concluded that this strategy is better than single-stage forming. Lu et al. [24] presented a feature-based tool path generation mechanism. They compared the results of surface quality, thickness distribution and geometric accuracy with conventional SPIF method and concluded that the new tool path generation mechanism provided better surface quality than the traditional method. Ambrogio et al. [25] introduced the strategies to enhance geometric accuracy with back drawing processes and with multi-stage tool path forming of a blank sheet.

However, there are challenges associated with SPIF technology for its use on an industrial scale due to the inconsistencies observed in the existing literature. This makes it

difficult for practitioners to choose the correct SPIF parameters for the fabrication of parts with desired shapes and adequate mechanical properties. For example, Cawley et al. [26] reported low formability of Al 3003-O by using flat end tools, contrary to that, Ziran et al. [13] demonstrated better formability and surface quality of the same material by using hemispherical tools. Similarly, Cawley et al. [26] examined that parabolic tools reduced formability, whereas inverse results of parabolic tools about formability were reported by Adams [27]. The surface roughness is an essential requirement in determining the quality of the product and widely used as an index of product quality.

1.1 Significance and Aim of Study

The quality and dimensional accuracy of forming components are currently of high interest. Therefore, the *literature gap* highlights the need to critically analyze the tools and other forming parameters to investigate their influence on the surface quality and geometry of the fabricated parts. The selection of material for this study is based on the literature gap. From the literature, it is observed that formability, surface quality, and its analysis have not been investigated for all aluminum alloys. Aluminum alloys such as AA 5052, 6061 and 2219 are widely used in the automotive and aerospace industry; therefore, AA 2219-O is considered in this work. Also, most of the researches utilized spiral path and unidirectional fixed tool path which offers a twisting mechanism [37]; therefore, to overcome this problem, a bidirectional fixed path is adopted in this study, which is the *novelty* of this research. Keeping in view the requirements, this study *aims* to systematically investigate the influence of critical parameters of SPIF process including feed rate (F), spindle speed (S), and step increment (D) for the fabrication of Al alloy (AA 2219-O) alloy and optimize surface roughness (R_a), maximum wall angle (α_{max}), % thickness reduction (% TR), and forming time (T). This investigation will *contribute* towards the support for manufacturers and industrial users to consider these factors and utilize the results of study to commercialize the SPIF process for AA 2219-O.

A summary of related literature on optimization of forming parameters using various techniques for Aluminum alloy is provided in Table 1.

In the next chapter, the experimental plan, experimental setup, material characteristics, forming tools, forming parameters utilized and process for each experiment was conducted for this study.

2 Research Methodology

Figure 1 shows the illustration of the methodology adopted in this study to systematically evaluate the influence of SPIF process on the forming ability of Al alloy (AA 2219-O).

Table 1 Summary of literature on fabrication of Aluminum alloy using SPIF

Material	Geometry	Experimentatal Design	Process parameters							Refs		
			Feed rate	Spindle speed	Sheet thickness	Tool types	Tool size	Step increment	Wall angle		Part depth	Geometry
AA-6061	Tubes	RSM, ANOVA	*	*								[20]
Al 1050	Pyramid	Taguchi RSM, ANOVA				*	*	*	*			[28]
Al 1100	Truncated Pyramid	Taguchi ANOVA	*	*				*	*			[29]
AL-1100	Conical	Taguchi ANOVA	*	*				*	*			[30]
AL-AA 5052	Simple straight shapes at 0, 45, 90 angle	Taguchi, ANOVA, GRA with PCA	*	*	*	*	*	*	*			[31]
AL 6061	Square part	Box-Benken, RSM	*	*								[32]
AL AA 1050	Cup shape	Taguchi, ANOVA, RSM, GRA	*	*	*	*	*	*	*			[33]
AL AA 8011	Cone shape	Desirability										[15]
AL AA 6061	truncated cone	Circle grid analysis Straight groove test, forming limit diagrams						*	*	*	*	[34]

Table 1 (continued)

Material	Geometry	Experimental Design	Process parameters							Refs		
			Feed rate	Spindle speed	Sheet thickness	Tool types	Tool size	Step increment	Wall angle		Part depth	Geometry
Al 3003-O	Cone	Variable wall angle step test (VWAST)	*	*					*			[26]
AL-AA 5052	Frustum of cone	Tensile test, CDD, RSM, ANOVA, ramp analysis	*	*					*			[35]
AL-AA 1050	Conical pyramid	Tensile test, microscopic thickens analysis	*		*	*	*	*	*	*	*	[36]
AA 2219	Truncated pyramid	CCD, RSM, ANOVA	*	*		*			*		*	Current study





Fig. 1 Research methodology to evaluate the effect of critical SPIF parameters on the forming of Al alloy (AA2219-O)

Table 2 Chemical composition and mechanical properties of AA 2219-O

Chemical composition (wt. %)									Tensile properties		
Al	Cu	Fe	Mg	Mn	Si	Ti	V	Zn	Ultimate tensile strength (MPa)	Elongation %	Young's modulus (GPa)
91.5–93.8	5.8	0.3	0.02	0.2	0.2	0.02	0.05	0.1	172	20	72

In this study, 1.5 mm thick Al alloy (AA 2219-O) plates were used with the initial dimensions of 150 × 150 mm (length × width). The chemical composition and tensile properties of AA 2219-O are summarized in Table 2.

Two types of forming stainless steel (SS) tools, i.e., flat end tool and a freely rotating ball tool with tool diameter of 10 mm were used for the fabrication of Al alloy sheets, as shown in Fig. 2a. Figure 2b shows the experimental setup on 3 axis CNC milling machine which includes clamping jig, forming tool and a blank. To perform incremental sheet metal forming operation Deckel Maho DMU 35 M CNC universal machining Center was used. For lubrication at tool-sheet interface, finarol refined oil of oil company TOTAL was used. In each experiment, the tool path was a truncated pyramid with a top-end diameter of 75 mm and the bottom end diameter of 30 mm, as shown in Fig. 2c. The spiral tool path strategy (STPS) was selected in this study instead of a fixed step increment (FSI) because STPS leaves no marks at the step down on the fabricated sheet metal.

2.1 Design of Experiments

Various qualitative and quantitative SPIF parameters and levels for the design of experiments (DOE) used in this study are summarized in Table 3. The range of levels for DOE is selected based on the available 3 axis CNC machine specifications which includes spindle speed range (20–6000 rpm) and feed rate (max. 5000 mm/min). The machine has a maximum drive motor of 7.5 kW, maximum stroke length of 765 mm × 450 mm × 450 mm in x , y and z directions, respectively. Due to a wide range of factors, central composite design (CCD) technique was used, which required fewer experiments to perform instead of full or fractional factorial experimental design. Design Expert 7.0 and Minitab software applications were used in this investigation. Twenty runs were designed for both forming tools using spiral forming path.

The experimental design matrix for the flat end tool is presented in Table 4. The 20 test points allow the estimation of the linear, quadratic, and two-way interactive effects of the forming factors. DOE for rotating ball with spiral and bi-directional trajectory is given separately in Appendix. The measured responses from the SPIF process were R_a , α_{max} , T , and % TR. The test points were run randomly to avoid any systematic error in the system. To measure R_a , profilometer (Surftest SJ-410) was used. R_a values of the fabricated parts were evaluated using [38]:

$$R_a = \frac{1}{L} \int_0^L |Y(x)| dx \quad (1)$$

Formability is measured by the bevel protector and coordinate measuring machine (CMM). Forming time was recorded when the machine started its forming operation up to that point when a crack occurred in the formed sheet. The final thickness of the sheet (t_f) was measured using a micro screw gauge with least count of 0.001 mm. TR values were evaluated using Eqs. 2 and 3.

$$t_f = t_0 \times \sin(90 - \alpha) \quad (2)$$

$$\%TR = \frac{t_0 - t_f}{t_0} \times 100 \quad (3)$$

where t_0 and α are the initial thickness and forming angle, respectively.

To develop the models, at least 60 specimens were fabricated and tested.

2.2 Empirical Modeling

In RSM usually, two types of models are developed as given below.

First-Order model as:

$$y = \beta_0 + \beta_1 x_1 + \beta_2 x_2 + \beta_k x_k + \epsilon \quad (4)$$

Second-Order model as:

$$y = \beta_0 + \sum_{i=1} \beta_i x_i + \sum \beta_{ii} x_i^2 + \sum_{i < j} \beta_{ij} x_i x_j + \epsilon \quad (5)$$

where y represents Response, mean of responses is termed as β_0 and the coefficient of responses are β_i , β_{ii} , β_{ij} . These coefficients depend on the interactions and main parameters. The coded independent variables are denoted as x_i , x_j . The simplified empirical models are shown in Eqs. 6–17

$$\begin{aligned} R_a (\text{Flat tool, spiral path}) = & + 16.38 - 0.012F - 3.704e^{-3}V \\ & + 1.036D - 1.60e^{-7}FV - 6.66e^{-5}FD \\ & + 6.67e^{-4}VD + 3.23e^{-6}F^2 \\ & + 1.97e^{-6}V^2 - 1.630D^2 \end{aligned} \quad (6)$$

$$\begin{aligned} R_a (\text{Ball tool, spiral path}) = & + 7.33 - 7.46e^{-3}F - 2.17e^{-3}V \\ & + 3.688D - 3.60e^{-7}FV \\ & - 6.67e^{-5}FD - 2.03e^{-3}VD \\ & + 2.0e^{-6}F^2 + 1.26e^{-6}V^2 - 1.281D^2 \end{aligned} \quad (7)$$

$$\begin{aligned} R_a (\text{Ball tool, bi-directional path}) = & + 11.51 - 6.4e^{-3}F - 9.63e^{-3}V \\ & - 0.838D + 9.19e^{-7}FV - 3.94e^{-5}FD \\ & + 4.19e^{-3}VD + 1.56e^{-6}F^2 \\ & + 3.64e^{-6}V^2 - 0.135D^2 \end{aligned} \quad (8)$$

$$\alpha_{max} (\text{Flat tool, spiral path}) = + 188.74 - 0.071F - 0.104V$$

Fig. 2 Tools, experimental setups, and strategies used for the fabrication of Al alloy sheets-**a** Flat end tool (left) and freely rotating ball tool (Right), **b** experimental setup, and **c** Truncated pyramid tool path

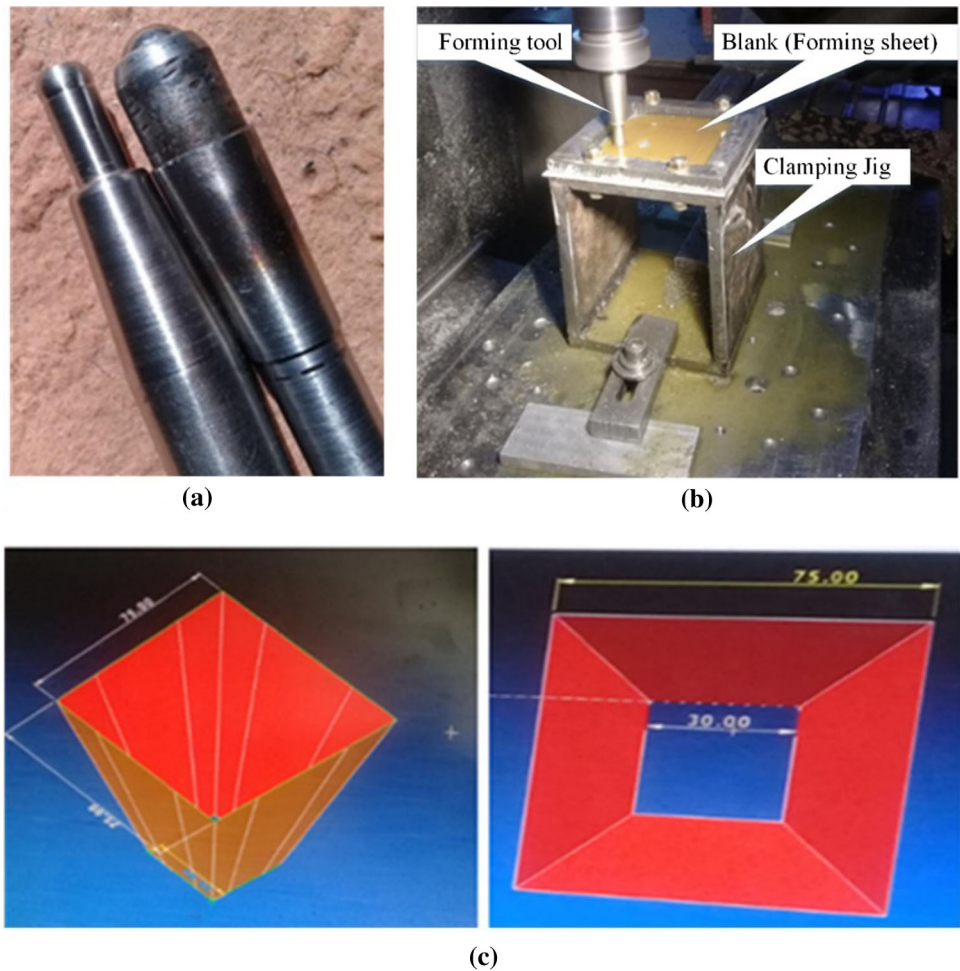


Table 3 SPIF parameters and their levels used for the forming of Al alloy sheets

Factors	Low level (1)	Medium level (0)	High level (1)
<i>Quantitative</i>			
Spindle speed (rpm)	450	700	950
Feed rate (mm/min)	1500	2000	2500
Step increment (mm)	0.3	0.6	0.9
<i>Qualitative</i>			
Forming tools	Flat end	Rotating ball end	N/A
Forming path	Spiral (Unidirectional)	Bidirectional	N/A

$$\begin{aligned}
 & -75.94D + 6.50e^{-6}FV - 0.013FD \\
 & + 3.167e^{-3}VD + 1.73e^{-5}F^2 \\
 & + 5.86e^{-5}V^2 + 74.09D^2 \quad (9)
 \end{aligned}$$

$$\begin{aligned}
 \alpha_{\max}(\text{Ball tool, spiral path}) = & + 21.79 + 0.059F \\
 & + 0.079 V - 101.093D \\
 & - 2.59e^{-5}FV - 6.25e^{-3}FD \\
 & + 0.057 VD - 1.11e^{-5}F^2
 \end{aligned}$$

$$\begin{aligned}
 \alpha_{\max}(\text{Ball tool, bi-directional path}) = & + 97.20 - 0.013F \\
 & - 0.027 V - 15.50D \\
 & + 1.47e^{-5}FV - 0.01FD \\
 & - 0.02 VD + 3.14e^{-6}F^2 \\
 & + 1.28e^{-6}V^2 + 29.17D^2 \quad (11)
 \end{aligned}$$

Table 4 DOE and corresponding responses for a flat end tool and spiral path

Run no.	Parameters		Coded parameters values			Performance measures			
	Path	Tool	<i>F</i> (mm/min)	<i>V</i> (rpm)	<i>D</i> (mm)	<i>R_a</i> (μm)	(<i>α_{max}</i>)	<i>T</i> (min)	% TR
1	Spiral	Flat	1500	450	0.3	3.74	68.2	25.33	49.6
2			2500	450	0.3	4.01	67	20.67	52.06
3			1500	950	0.3	3.45	61.5	13.33	51.4
4			2500	950	0.3	3.65	62.2	17.5	56.2
5			1500	450	0.9	3.27	64.5	5.7	50.5
6			2500	450	0.9	3.49	53.8	14.33	59.2
7			1500	950	0.9	3.19	57.4	9.67	55.3
8			2500	950	0.9	3.34	51.3	19.5	60
9			1159.1	700	0.6	4.56	65.5	10.67	51.6
10			2840.8	700	0.6	5.18	54.3	16.47	61.5
11			2000	279.55	0.6	3.54	59.5	22.62	52
12			2000	1120.4	0.6	2.32	56.5	17.21	54.2
13			2000	700	0.10	2.41	71.6	20.35	43.2
14			2000	700	1.10	1.92	61.4	10.53	50.3
15			2000	700	0.6	2.41	50.2	15.7	43.7
16			2000	700	0.6	2.75	46.7	16.18	47.2
17			2000	700	0.6	2.70	47.3	14.25	46.7
18			2000	700	0.6	2.75	41.6	12.5	47
19			2000	700	0.6	2.71	49.5	13.65	47.2
20			2000	700	0.6	2.73	44.7	12.2	47.06

Table 5 Summary of ANOVA for all variables

Response	Tool	Path	Model	Terms									<i>R</i> ²	Adj <i>R</i> ²	Pred. <i>R</i> ²	
				F	V	D	FV	FD	VD	F ²	V ²	D ²				
Ra	Flat	Spiral	Adequate	*	*	*					*	*	*	0.9655	0.9344	0.7823
	Ball	Spiral	Adequate	*	*	*				*	*	*	0.9582	0.9205	0.7285	
	Ball	Bi-dir	Adequate	*	*	*	*			*	*	*	0.9675	0.9193	0.7430	
(<i>α_{max}</i>)	Flat	Spiral	Adequate	*	*	*	*	*			*	*	*	0.9439	0.8934	0.7981
	Ball	Spiral	Adequate	*	*	*	*			*	*	*	0.9357	0.8778	0.7028	
	Ball	Bi-dir	Adequate	*	*	*	*			*	*	*	0.9509	0.9067	0.7914	
%TR	Flat	Spiral	Adequate	*	*	*	*	*			*	*	*	0.9948	0.9901	0.9687
	Ball	Spiral	Adequate	*	*	*					*	*	0.9470	0.8994	0.6967	
	Ball	Bi-dir	Adequate	*	*	*					*	*	*	0.9539	0.9124	0.7612
T	Flat	Spiral	Adequate	*	*	*	*	*	*			*	0.9389	0.8838	0.6989	
	Ball	Spiral	Adequate	*	*	*	*	*	*			*	0.9384	0.8829	0.7114	
	Ball	Bi-dir	Adequate	*		*					*	*	*	0.9346	0.8757	0.6234

$$\begin{aligned}
 \% \text{ TR}_{(\text{Flat tool, spiral path})} &= + 118.5 - 0.059F && + 4.34e^{-5}V^2 + 5.34D^2 && (12) \\
 &- 0.052 V - 9.347D \\
 &- 1.73e^{-6}FV + 5.11e^{-3}FD \\
 &- 6.67e^{-4}VD + 1.57e^{-5}F^2 \\
 \% \text{ TR}_{(\text{Ball tool, spiral path})} &= + 73.29 - 0.022F \\
 &- 0.01 V + 0.94D \\
 &- 2.60e^{-6}FV - 2.83e^{-3}FD
 \end{aligned}$$

$$\begin{aligned}
 &+ 1.22e^{-4}VD + 7.08 F^2 \\
 &+ 1.02e^{-5}V^2 + 2.668D^2 \quad (13)
 \end{aligned}$$

$$\begin{aligned}
 \% TR_{(Ball\ tool,\ bi-directional\ path)} = &+ 127.91 - 0.071F \\
 &- 0.068V - 19.60D \\
 &- 1.73e^{-6}FV + 5.11e^{-3}FD \\
 &- 6.67e^{-4}VD + 1.88 F^2 \\
 &+ 5.48e^{-5}V^2 + 13.856D^2 \quad (14)
 \end{aligned}$$

$$\begin{aligned}
 T_{(Flat\ tool,\ spiral\ path)} = &+ 76.71 - 7.22e^{-3}F \\
 &- 0.091V - 75.91D \\
 &+ 1.003e^{-5}FV + 0.015FD \\
 &+ 0.04VD - 1.303e^{-6}F^2 \\
 &+ 3.06e^{-5}V^2 + 3.725D^2 \quad (15)
 \end{aligned}$$

$$\begin{aligned}
 T_{(Ball\ tool,\ spiral\ path)} = &+ 81.47 - 7.30e^{-3}F \\
 &- 0.090V - 77.32D \\
 &+ 9.41e^{-6}FV + 0.016FD \\
 &+ 0.04VD - 1.27e^{-6}F^2 \\
 &+ 3.05e^{-5}V^2 + 3.797D^2 \quad (16)
 \end{aligned}$$

$$\begin{aligned}
 T_{(Ball\ tool,\ bi-directional\ path)} = &- 12.23 + 0.05F \\
 &+ 0.062V - 75.10D \\
 &+ 1.00e^{-5}FV + 0.01FD \\
 &+ 2.83e^{-4}VD - 1.77e^{-5}F^2 \\
 &- 5.04e^{-5}V^2 + 24.39D^2 \quad (17)
 \end{aligned}$$

Subjected to constraints

$$1500 \leq F \leq 2500$$

$$450 \leq V \leq 550$$

$$0.3 \leq D \leq 0.9$$

2.3 Model Validity

For model validity and significance of model terms, ANOVA was applied. The results of ANOVA are shown in Table 5. It is found that the calculated F-ratios of developed models are larger than the standard F-ratio at a 95% confidence level ($F_{0.05}(9, 10) = 3.02$); hence, the models are considered to be adequate. Furthermore, the F-ratios also indicate the significance of the model terms. The higher F-ratio corresponds to the larger effect of the term on the model response. To increase model accuracy, the standard ratio $F_{0.10}(1, 10) =$

Table 6 Validation experiments

Run	Feed rate (mm/min)	Spindle Speed (rpm)	Step increment (mm)	Surface roughness (µm)			Wall angle (degree)			Thickness reduction (%)			Forming time (min)			
				Setup	A	B	C	A	B	C	A	B	C	A	B	C
1	1700	500	0.7	Actual	2.98	2.47	2.29	52.76	59.87	67.87	48.75	45.82	38.71	12.64	20.73	19.73
				Pred	3.03	2.42	2.262	54.02	58.17	66.42	50.05	47.56	37.19	13.15	20.12	20.66
				%E	1.55	2.27	1.59	2.33	2.93	2.19	2.60	3.66	4.09	3.88	3.03	4.50
2	1900	600	0.5	Actual	2.72	2.22	2.05	52.12	61.45	64.28	51.27	43.47	33.21	15.52	21.67	26.98
				Pred	2.82	2.18	1.98	50.67	64.38	67.31	49.81	45.45	34.48	16.21	20.97	27.25
				%E	3.57	1.69	3.38	2.86	4.55	4.50	2.93	4.36	3.68	4.26	3.34	0.99
3	2200	750	0.7	Actual	2.93	2.55	2.09	43.28	53.65	65.76	52.45	51.35	40.2	13.65	18.64	19.7
				Pred	2.85	2.51	2.14	45.47	55.78	63.88	50.45	49.32	38.32	14.29	19.11	20.6
				%E	2.77	1.51	2.15	4.82	3.82	2.94	3.96	4.12	4.91	4.48	2.41	4.37
4	2400	800	0.8	Actual	2.95	2.83	2.47	45.23	48.73	58.5	52.43	53.21	45.54	16.14	19.41	15.76
				Pred	3.05	2.81	2.56	47.11	50.95	60.28	51.65	53.89	43.64	15.55	20.22	16.08
				%E	3.05	0.71	3.7	3.83	4.36	2.95	1.51	1.28	4.35	3.79	4.06	1.99
5	2200	500	0.5	Actual	2.93	2.31	2.14	48.24	53.45	64.52	53.23	50.32	39.16	17.82	21.79	20.82
				Pred	3.06	2.28	2.12	50.28	55.84	63.66	51.41	48.34	37.82	18.18	22.56	21.23
				%E	4.47	1.23	0.7	4.06	4.28	1.35	3.54	4.05	3.54	1.98	3.81	1.93

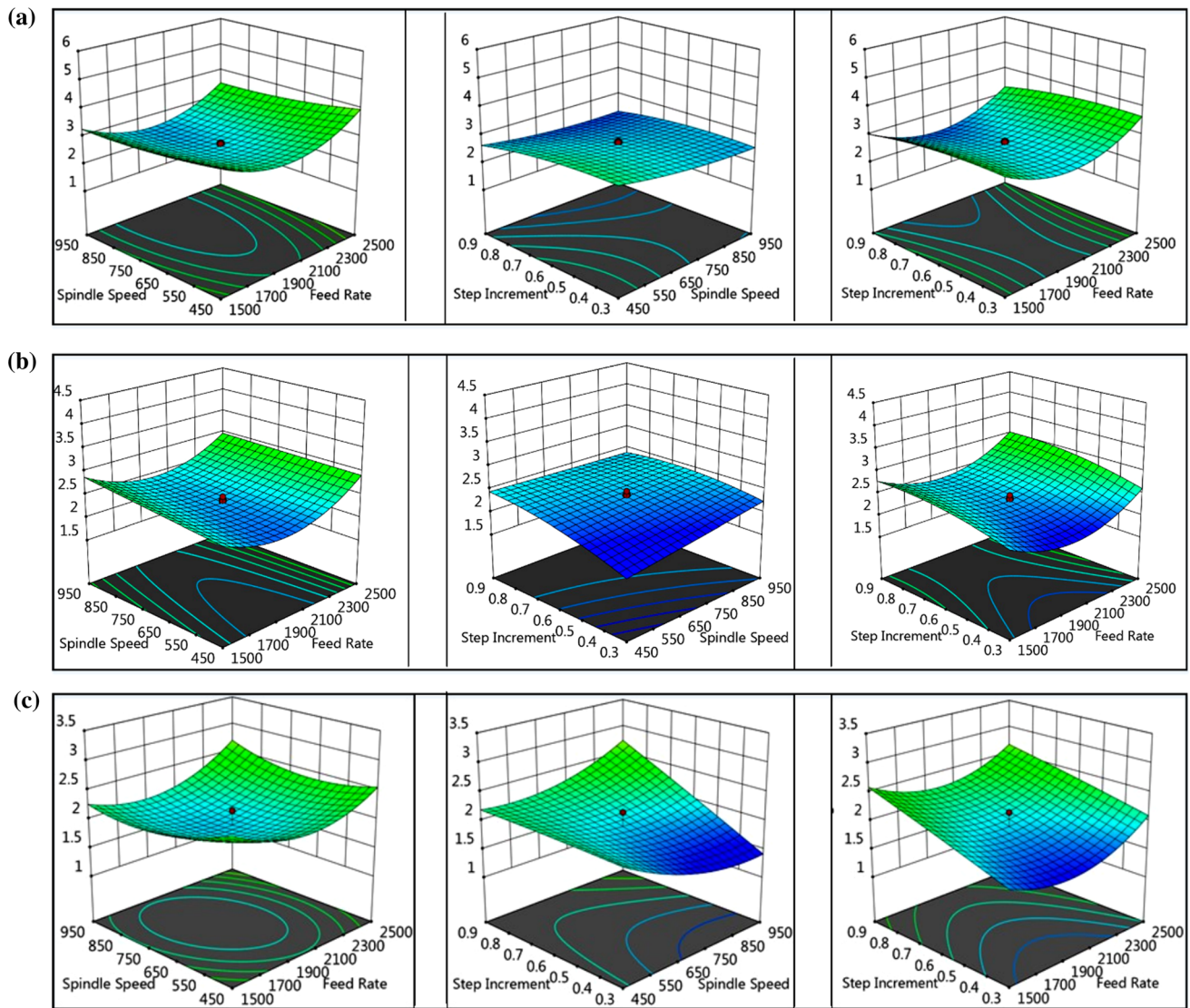


Fig. 3 3D plots of surface roughness of the fabricated SPIF parts **a** flat end tool and spiral path, **b** ball end tool and spiral path, and **c** ball end tool and bi-directional path

3.29 is set as the criterion of significance. Table 5 summarizes the results of all experimental setups. The terms with the F-ratios larger than 3.29 are defined as significant terms and marked * in the remarks column of Table 5. For example, in the first experimental setup with flat tool and spiral tool path to measure R_a , significant factors include feed rate (F), speed (V), step increment (D) and F^2 , V^2 , and D^2 . Likewise, all the results are mentioned in Table 5.

The validity of the simplified models is further tested by the coefficient of determination R^2 , which indicates how well a model fits the data. $R^2 = 1$ means that the empirical model fits data perfectly, while $R^2 = 0$ indicates that the model does not fit the data at all. For the proposed models the calculated R^2 values are listed in Table 5. As all the R^2 values are nearly

equal to 1, this shows that Eqs. 6–17 describe the relationships between forming factors and responses very well.

Furthermore validation experiments were also conducted using flat end tool and spiral path (represented as A in the table), and ball end tool using spiral path (represented as B), and with ball end tool using bidirectional path (represented as C). The values on which the validation experiments were performed were within the designed parameters range. Percentage error between actual and predicted values is calculated using Eq. 18 below. The results are presented in Table 6 below and the calculated error is less than 5%.

$$\% E = \left| \frac{\text{actual value} - \text{predicted value}}{\text{predicted value}} \right| \times 100 \quad (18)$$

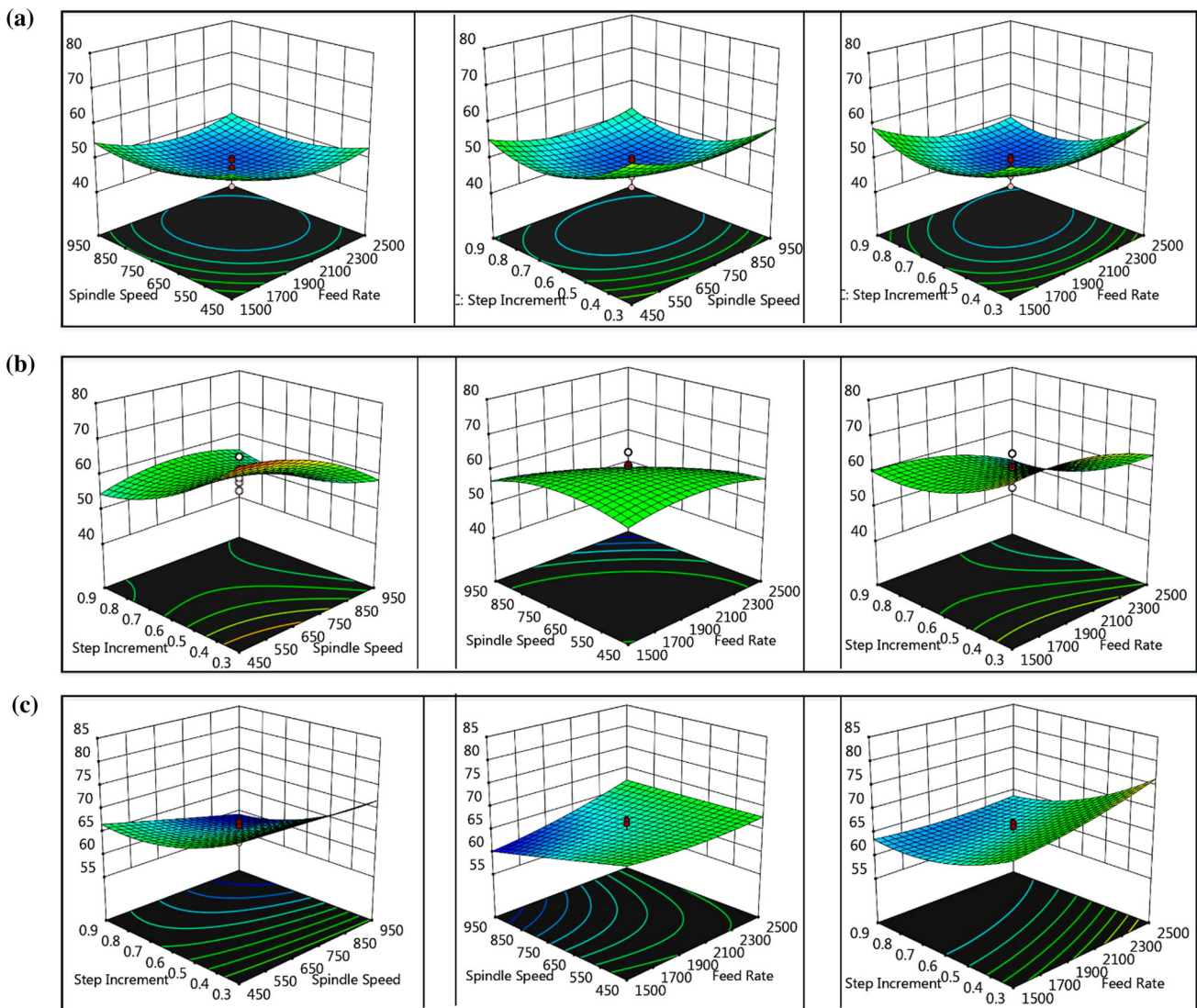


Fig. 4 3D plots of maximum wall angle **a** flat end tool and spiral path, **b** ball end tool and spiral path, and **c** ball end tool and bi-directional path

3 Results and discussion

3.1 3D Response Graphs

3.1.1 The Surface Roughness of Fabricated Parts

Figure 3 represents the relationship between feed rate, spindle speed, step increment on the surface finish produced by the flat end and ball end tools using spiral and bi-directional paths. For flat tool and spiral path, Fig. 3a shows that surface roughness (R_a) decreases to $2.7 \mu\text{m}$ by increasing the feed rate up to 1995 mm/min. After $2.7 \mu\text{m}$ R_a increases with the increase in the feed rate. Also, R_a decreases by increasing spindle speed. The same relationship is observed in R_a and

step increment. With the ball end tool using a spiral path (Fig. 3b), R_a decreases to $2.214 \mu\text{m}$ by increasing feed rate up to 2005 mm/min and spindle speed 689.89 rpm. After that limit, it increases. In the case of the ball-end tool using a bi-directional path (Fig. 3c), R_a decreased to $1.9579 \mu\text{m}$ by increasing the spindle speed up to 823.13 rpm and feed rate up to 1838.28 mm/min. After that limit, R_a increased by increasing the cutting speed and feed rate. From these results, it can be seen that R_a of the formed sheets strongly depends upon the feed rate during the SPIF process. Moreover, the effect of feed rate and spindle speed on the surface roughness of the parts stays similar in three conditions. However, in the case of step increment, R_a increases by increasing the step increment.

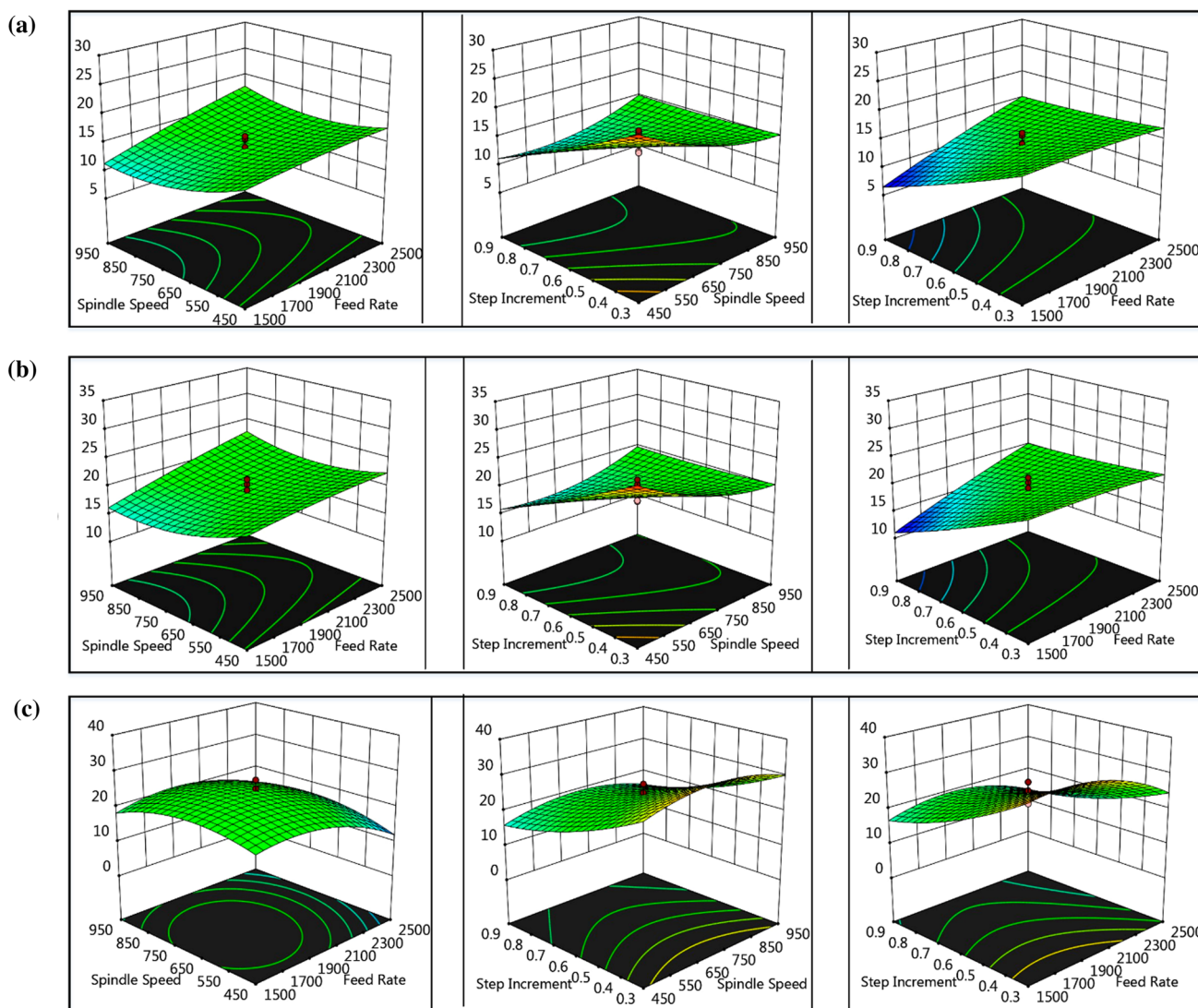


Fig. 5 3D response graphs of Forming time **a** flat end tool and spiral path **b** ball end tool and spiral path **c** ball end tool and bi-directional path

3.1.2 Maximum Wall Angle

Figure 4 shows the 3D plots of F , V and D and their effects on the maximum wall angle. With a flat end tool using a spiral path (Fig. 4a), α_{\max} decreases up to 46° by increasing the spindle speed 698 rpm and feed rate up to 2000.1 mm/min and step increment of 0.6 mm. After 46° , α_{\max} increases with further increase in the parameters. With the ball end tool using a spiral path (Fig. 4b), α_{\max} increases up to 61° by increasing the spindle speed 700.06 rpm and feed rate up to 1990.95 mm/min. After 61° , α_{\max} decreases. α_{\max} shows sensitive behavior towards step increment as a small increment significantly affects wall angle. Figure 4c shows the variation of α_{\max} with a ball end tool using a bidirectional path. It can be seen that spindle speed has the inverse relationship and feed rate has a direct relationship with α_{\max} . α_{\max} decreases

by increasing the spindle speed and decreasing the feed rate. α_{\max} shows more sensitivity towards the spindle speed. In the case of step increment, α_{\max} increases by decreasing the step increment.

3.1.3 Forming Time

The comparison of forming tools and forming paths in Fig. 5 reveals that for the flat end and ball end tools, spindle speed shows a similar behavior towards the forming time (T). Figure 5a shows the results of the flat tool with a spiral path. It shows that T has a direct relation with feed rate and inverse relation with step increment, whereas T decreases to 14.5 min by increasing spindle speed up to 700 rpm. Further increase in speed has a very slight effect on T . Feed rate shows more sensitivity towards the forming time than the spindle speed.

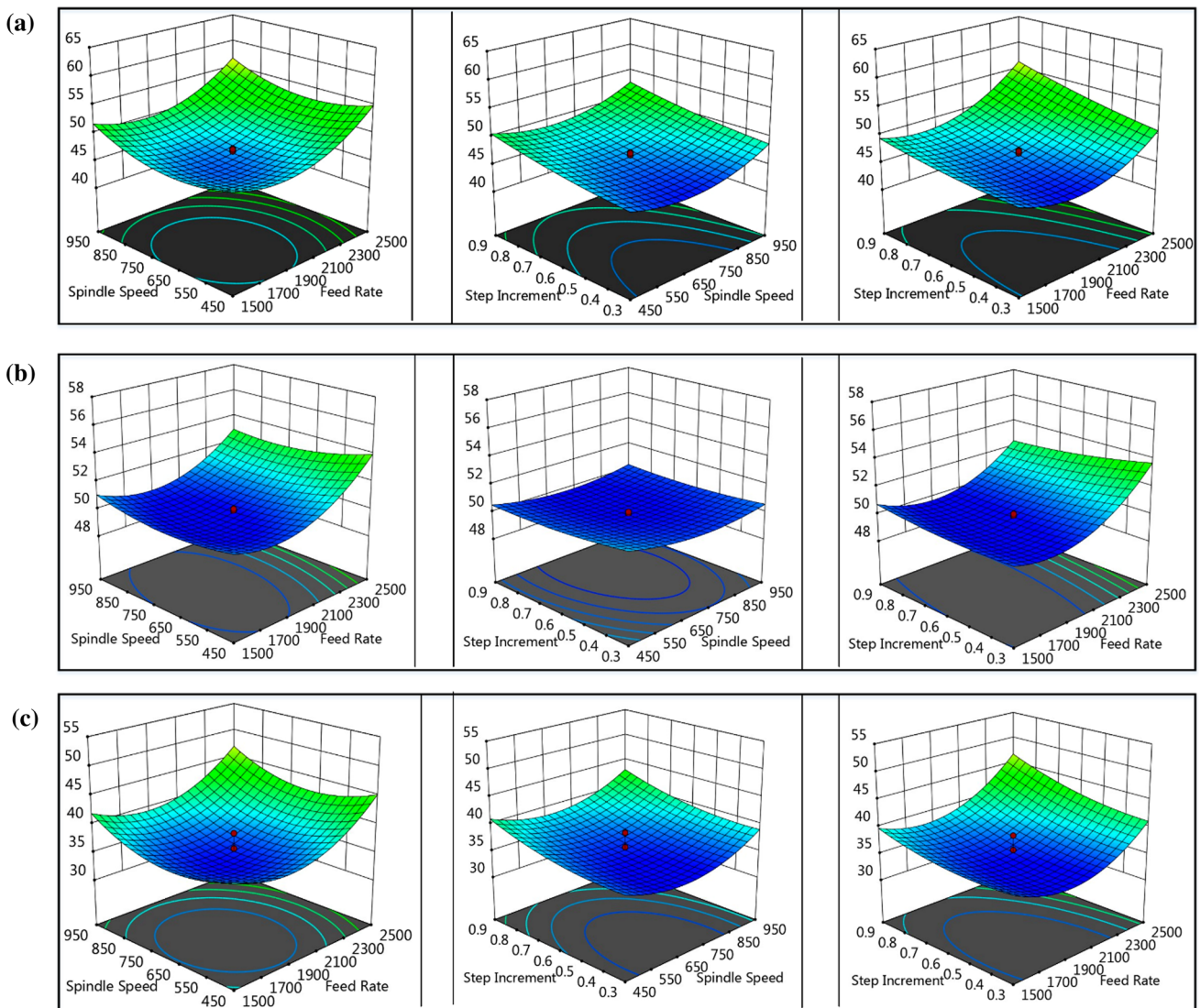


Fig. 6 3D plots of %thickness reduction **a** flat end tool and spiral path, **b** ball end tool and spiral path, and **c** ball end tool and bi-directional path

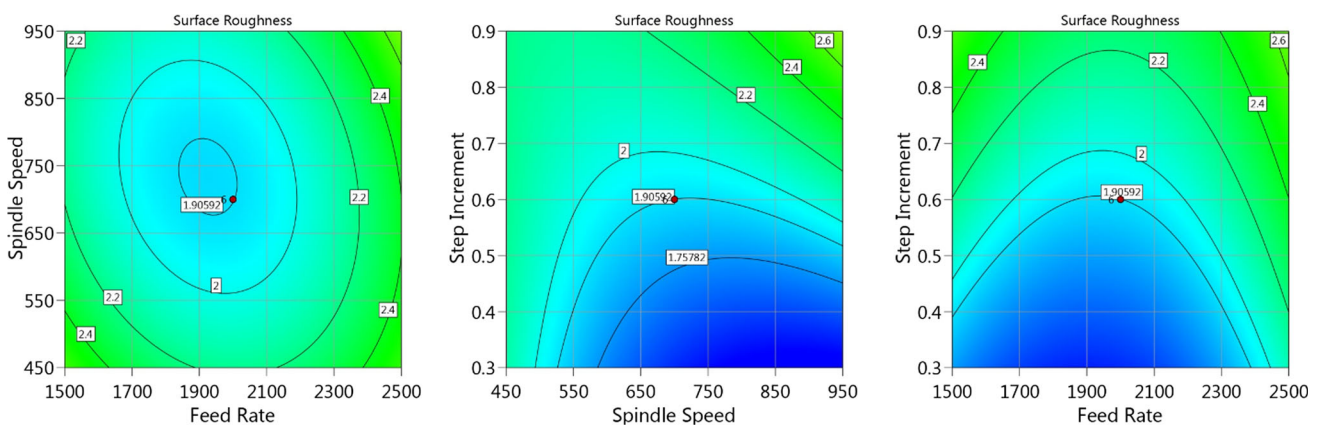


Fig. 7 Contour plots of surface roughness

Fig. 8 Contour plots of Wall Angle

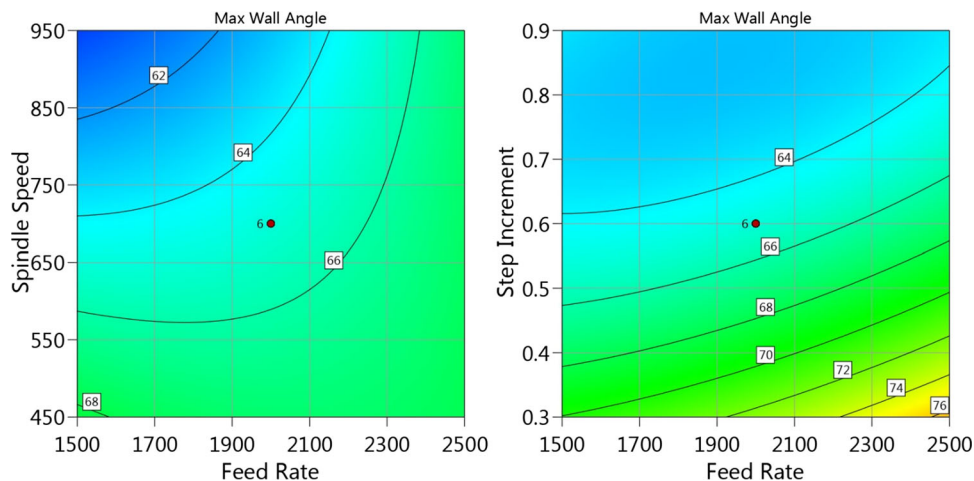
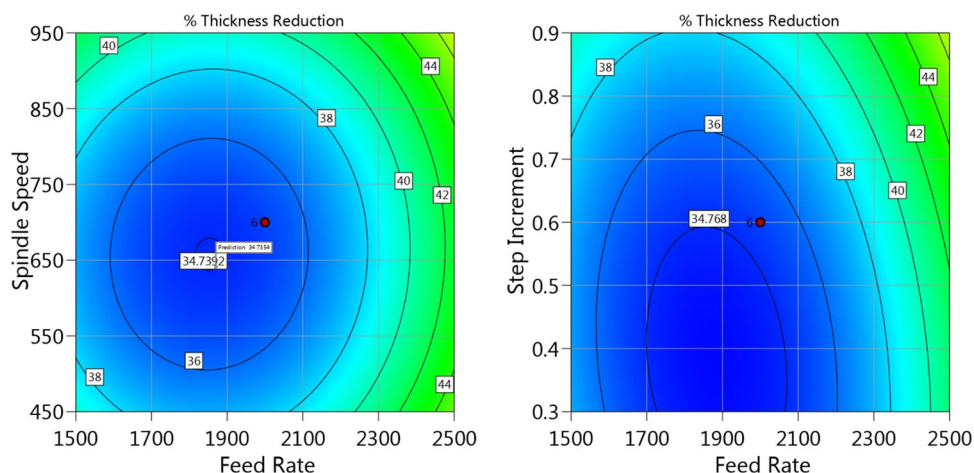


Fig. 9 Contour plots of % thickness reduction



A similar relationship is found with a ball tool and spiral path experimentation as shown in Fig. 5b. Figure 5c shows that T increases by increasing the spindle speed up to 702.78 rpm and feed rate up 1999.86 mm/min. After 25 min, T decreases by increasing the spindle speed and feed rate. Forming time shows more sensitivity toward the feed rate. The results show that the behavior of step increment is in three conditions. In the case of step increment, forming time decreases by increasing the step increment.

3.1.4 % Thickness Reduction

Figure 6 shows the results of % TR with a flat end tool using a spiral path and ball end tool using both spiral and bidirectional paths. In the case of flat end tool using a spiral path (Fig. 6a), % TR first decreases up to 46% by increasing feed rate up to 1788.42 mm/min and spindle speed up to 590.53 rpm. Further increase in the parameters increases the %TR, whereas step increment has a direct relation with the %TR. With the ball end tool using a spiral path (Fig. 6b), % TR also decreases up to 49% with an increase in feed rate

up to 1806.6 mm/min. Further increase in feed rate significantly affect %TR. Likewise, an increase in spindle speed up to 730 rpm decreases %TR up to 49%. Further increase in speed increases the % TR. Figure 6c shows that using the ball tool with a bidirectional path, %TR decreases to 35% by increasing feed rate to 2000 mm/min and spindle speed to 700 rpm. Further increase in feed rate and spindle speed decreases %TR. However, for step increment, %TR increases with an increase in the step increment.

3.2 Comparison of Performance Measures Between Flat End and Ball Tool

The responses of R_a , α_{max} , T , and % TR using flat end and ball tool are compared and the analysis shows that the ball end tool had 19% times smaller R_a as compared to the flat end tool. Ball end tool had 16% times higher α_{max} as compared to the flat end tool. Flat end tool had 16% times higher % TR as compared to the ball end tool and flat end tool had 6% higher T than ball end tool.

Fig. 10 Contour plots of forming time

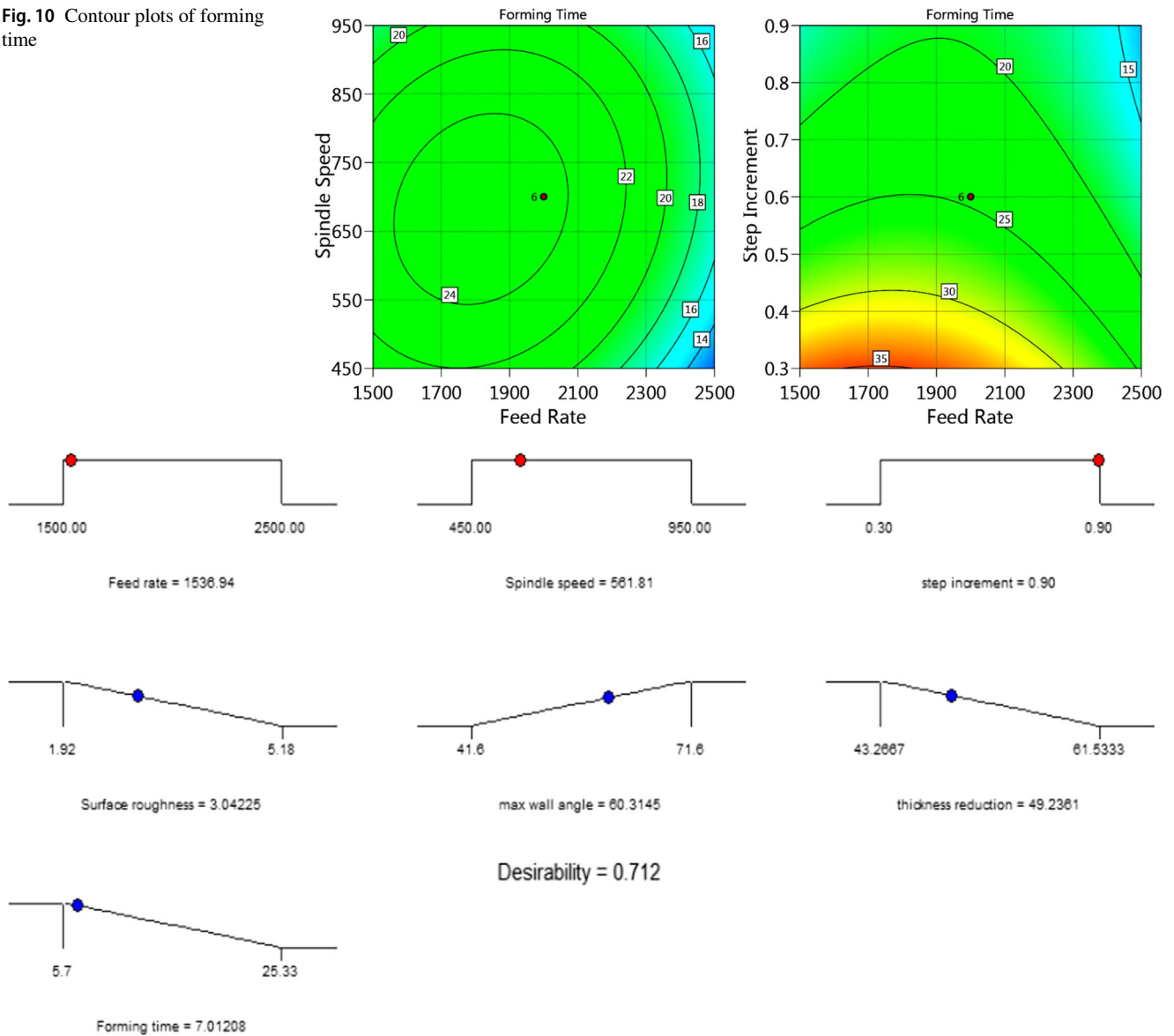


Fig. 11 Achievable range for observed performance measures using flat tool and spiral path

Likewise, when the responses of R_a , α_{max} , T, and % TR using spiral and bi-directional paths are compared the results showed that ball end tool using bidirectional path resulted in 17%, 18%, 19% and 35% reduction in R_a , α_{max} , % TR, and T, respectively.

3.3 Model Optimization

The significant parameters confirmed by ANOVA results were optimized to get minimum R_a , α_{max} , T, and % TR. Since the rotating ball end tool using a bidirectional path was best-suited SPIF parameters, therefore, only this experimental setup was optimized using the contour plots.

Figure 7 shows that the $1.905 \mu m R_a$ can be achieved at the feed rate of 1928 mm/min and a spindle speed of 672 rpm. A target R_a value of $1.905 \mu m$ can be achieved at feed rate 1912 mm/min and step increment of 0.61 mm. Similarly, R_a value of $1.76 \mu m$ can be achieved at a spindle speed of 748 rpm and a step increment of 0.49 mm. Similar target R_a values can be achieved on the other combinations within the design space that would ensure maximum productivity without any compromise on the desired surface finish.

Figure 8 shows that a $68^\circ \alpha_{max}$ can be achieved at a feed rate of 1558 mm/min and a spindle speed of 456 rpm. Likewise, target α_{max} value of 74° can be achieved by setting the feed rate 2260 mm/min and step increment at 0.370 mm. Similar target wall angle value can be achieved on the other

combinations within the design space that would ensure the maximum productivity without any compromise on desired product quality.

Figure 9 shows that the target % TR of 34.74% can be achieved at feed rate 1882.2 mm/min and a spindle speed of 675 rpm. And the target % TR value of 34.73 can be achieved by setting the feed rate at 1882 mm/min and step increment at 0.58 mm.

Figure 10 shows that 14 min forming time can be achieved at a feed rate of 2353 mm/min and a spindle speed of 490 rpm. Likewise, 15 min forming time can be achieved by setting the feed rate as 2369 mm/min and a step increment at 0.33 mm. A similar target T value can be achieved on the other combinations within the design space.

3.4 Optimization for Observed Responses using Desirability Index

The ramp plots were used to analyze the results obtained for numerical optimization of R_a , α_{max} , T , and % TR. Desirability is an objective function that ranges from zero outside of the limits to one at the goal [11]. The numerical optimization finds a point that maximizes the desirability function. For several responses and factors, all goals get combined into one desirability function.

The corresponding values of process parameters and performance measures for different conditions using a flat end tool and spiral path are presented in Fig. 11. It can be observed

that achievable maximum desirability of 71%, 2.5 μm of surface roughness, 60.3° of wall angle, % TR of 49% and forming time 7 min can only be achieved at different values of input parameters.

Similarly, for the maximum desirability of 73% using a ball tool and spiral path, 2.47 μm of surface roughness, 60.5° of wall angle, % TR of 49.8% and forming time 27.16 min can only be achieved at different values of feed rate, step increment, and spindle speed as shown in Fig. 12.

Similarly, for maximum desirability of 63% using a ball tool and bi-directional path, 1.85 μm of surface roughness, 75° of wall angle, % TR of 39.6% and forming time 27.16 min can only be achieved at different values of input parameters (Fig. 13).

4 Conclusion

Empirical models are developed to describe the relationships between the SPIF factors (feed rate, speed, step increment) on R_a , α_{max} , T , and % TR for aluminum alloy AA 2219-O. RSM, along with ANOVA, is utilized for the experimental validation of models. The result shows that the ball tool with a bi-directional path provides the most desired qualities. Furthermore, step increment is the most significant parameter in SPIF. The contour plots are utilized for the optimization of process parameters to achieve the desired values of output variables. The results suggest that among the forming

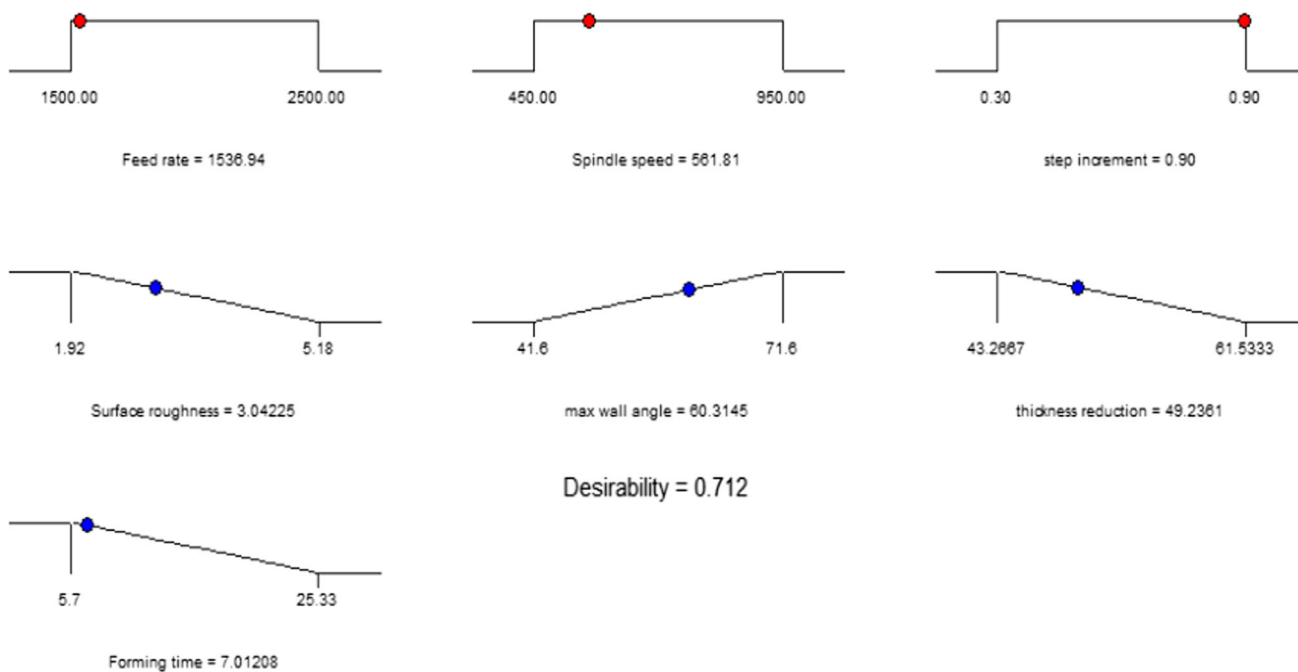


Fig. 12 Achievable range for observed performance measures using a ball tool and a spiral path

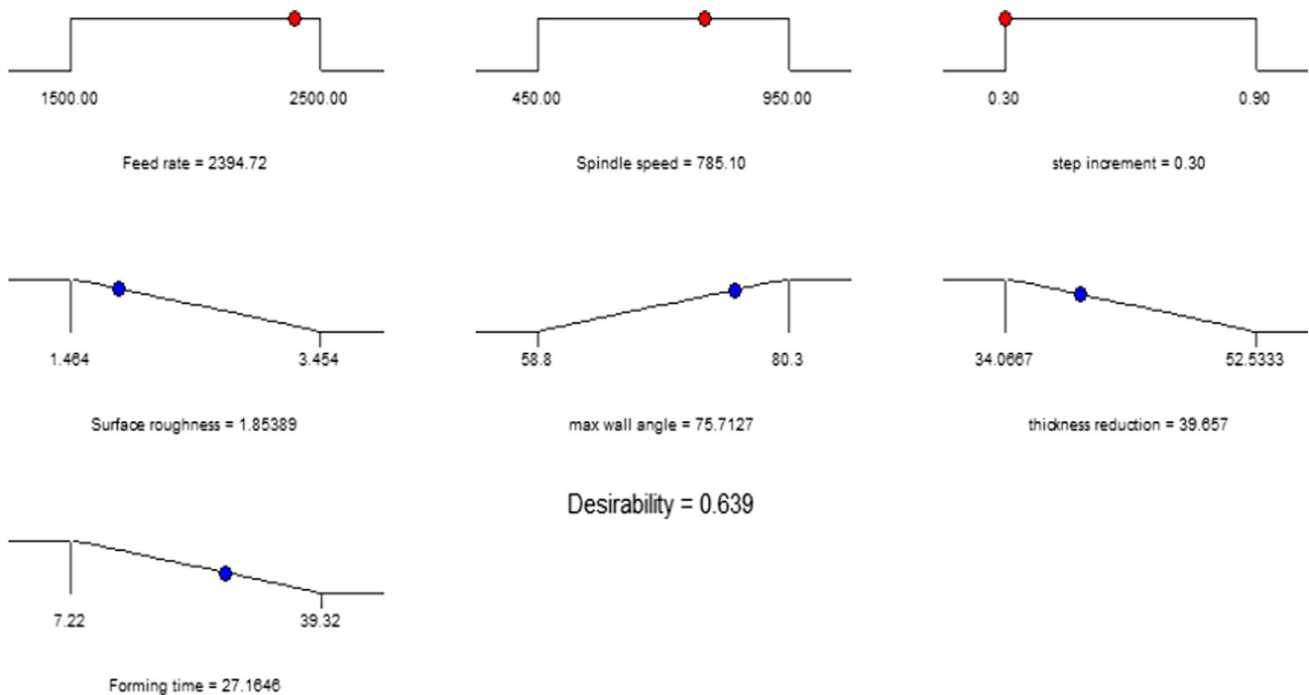


Fig. 13 Achievable range for observed performance measures using a ball tool and a spiral path

parameters in SPIF, step increment shows the most significant behavior regarding surface roughness, maximum wall angle and forming time and % TR in all three experimental setups.

Ball end tool has higher formability; better sheet thickness distribution and better surface finish than flat end tool. Moreover, it is observed that using a bidirectional forming path, forming force distributes homogeneously along the edge of geometric shape and increases the geometric accuracy of forming parts.

R_a increases with the increase in step increment. R_a with a flat end tool using a spiral path is high as compared to a ball end tool using both spiral and bidirectional path.

Flat end tool using a spiral path decreases wall angle with the increase in step depth, spindle speed and feed rate up to some extent after this wall angle increased, while, with the ball end tool using a spiral path, wall angle increases by an increase in spindle speed and feed rate up to some extent. After that limit wall angle decreases with the increase in the spindle speed and feed rate.

With the ball end tool using a bidirectional path, spindle speed and feed rate have the inverse behavior toward the wall angle. The wall angle shows more sensitive behavior toward spindle speed. In the case of step increment, the wall angle increases with the decrease in step increment.

In the case of step increment, forming time decreases with the increase in step increment. Moreover, forming time is independent of tool rotation speed. However, feed rates combined with step increment affect the forming time.

% TR decreases with an increase in feed rate up to some extent. After that limit, % TR increases with the increase in the feed rate. Moreover, % TR decreases by an increase in spindle speed up to some extent. However, in the case of step increment, % TR increases with the increase in step increment.

This study contributes a systematic insight into the influence of various complex SPIF parameters on the surface quality, wall angle and thickness distribution for the fabrication of an Al alloy sheet. This information could be extensively applied to a further design of the process control system to predict and control the surface quality of final parts manufactured by ISF. It is proposed that beyond simple shapes, SPIF can be applied for forming complicated shapes. If it is not possible to apply 100%, the aid of another forming process can be integrated with SPIF to reduce forming time and improve the part geometry and surface quality. Moreover, cost and productivity factors can also be included in the future research to enhance the practical significance of proposed work.

Author contributions UK was involved in methodology, resources collection, investigation, data curation and formal analysis. MHA was

involved in conceptualization, supervision and project administration. SQ was involved in software, writing—original draft and visualization. KM was involved in validation and writing—review and editing.

Funding This research did not receive any specific grant from funding agencies in the public, commercial, or not-for-profit sectors.

Availability of data and material The datasets generated during and/or analyzed during the current study are available from the corresponding author on reasonable request.

Code availability (software application or custom code) Not applicable.

Declarations

Conflicts of interest The authors have no conflict of interests. The authors also state that they have full control of all primary data and that they agree to allow the journal to review their data if requested.

Appendix

See Tables 7 and 8

Table 7 DOE and corresponding responses for a rotating tool and spiral path

Run no	Parameters		Coded parameters values			Performance measures			
	Path	Tool	Feed rate (mm/min)	Spindle Speed (rpm)	Step increment (mm)	Surface Roughness (μm)	Maximum wall angle	Forming time (min)	% TR
1	Spiral	Rotating ball	− 1	− 1	− 1	2.081	72.3	30.21	51
2			1	− 1	− 1	2.323	75.7	25.47	55.1
3			− 1	1	− 1	2.582	63.2	18.52	51
4			1	1	− 1	2.572	49.5	22.25	53.9
5			− 1	− 1	1	2.879	53.2	10.12	51.1
6			1	− 1	1	3.191	48.7	19.17	53.6
7			− 1	1	1	2.892	57.1	14.34	51.6
8			1	1	1	2.914	43.8	24.33	52.6
9			− 1	0	0	3.476	58.5	15.21	52.5
10			1	0	0	4.081	46.2	21.51	56.8
11			0	− 1	0	2.143	55.3	27.23	51.6
12			0	− 1	0	2.625	45.5	22.11	51.2
13			0	1	1	1.919	78.1	25.17	50.5
14			0	1	1	2.152	65.3	15.29	50.1
15			0	1	0	2.214	61.7	20.38	49.8
16			0	1	0	2.356	65.2	21.26	49.6
17			0	1	0	2.458	57.9	19.34	50
18			0	1	0	2.371	61.4	17.47	49.6
19			0	1	0	2.341	55.5	17.28	49.9
20			0	1	0	2.235	59.2	17.45	49.7

Table 8 DOE and corresponding responses for a flat end tool and bi-directional path

Run no	Parameters		Coded parameters values			Performance measures			
	Path	Tool	Feed rate (mm/min)	Spindle speed (rpm)	Step increment (mm)	Surface roughness (μm)	Maximum wall angle (Formability) degree	Forming time (min)	% TR
1	Bi-directional	Rotating ball	-1	-1	-1	2.257	72.4	35.4	40.6
2			1	-1	-1	2.563	74.3	18.78	43
3			-1	1	-1	1.552	67.2	29.5	42.4
4			1	1	-1	1.965	79.3	25.28	47.2
5			-1	-1	1	2.724	67.4	11.67	41.5
6			1	-1	1	2.441	65.9	9	50.2
7			-1	1	1	2.925	58.8	13.22	46.3
8			1	1	1	3.454	61.8	8.25	51
9			-1	0	0	2.925	65.4	16	42.6
10			1	0	0	3.173	69.4	7.22	52.5
11			0	-1	0	2.741	70.5	14.27	43
12			0	-1	0	2.433	60.3	13	45
13			0	1	1	1.464	80.3	39.2	34.2
14			0	1	1	2.352	64.9	21.38	41.5
15			0	1	0	2.151	66.4	27.62	35.7
16			0	1	0	1.833	63.8	21.5	34.5
17			0	1	0	1.827	67.2	23.39	34
18			0	1	0	1.842	63.7	25.23	34.4
19			0	1	0	1.889	62.6	22	34.6
20			0	1	0	1.874	66.3	27.67	38.4

References

- Park, J.-J.; Kim, Y.-H.: Fundamental studies on the incremental sheet metal forming technique. *J. Mater. Process. Technol.* **140**(1–3), 447–453 (2003)
- Emmens, W.; van den Boogaard, A.H.: An overview of stabilizing deformation mechanisms in incremental sheet forming. *J. Mater. Process. Technol.* **209**(8), 3688–3695 (2009)
- Dai, K.; Wang, Z.; Fang, Y.: CNC incremental sheet forming of an axially symmetric specimen and the locus of optimization. *J. Mater. Process. Technol.* **102**(1–3), 164–167 (2000)
- Wang, Z.; Cai, S.; Chen, J.: Experimental investigations on friction stir assisted single point incremental forming of low-ductility aluminum alloy sheet for higher formability with reasonable surface quality. *J. Mater. Process. Technol.* **277**, 116488 (2020). <https://doi.org/10.1016/j.jmatprotec.2019.116488>
- Shrivastava, P.; Tandon, P.: Microstructure and texture based analysis of forming behavior and deformation mechanism of AA1050 sheet during single point incremental forming. *J. Mater. Process. Technol.* **266**, 292–310 (2019)
- Zhang, Q.; Xiao, F.; Guo, H.; Li, C.; Gao, L.; Guo, X.; Han, W.; Bondarev, A.: Warm negative incremental forming of magnesium alloy AZ31 sheet: new lubricating method. *J. Mater. Process. Technol.* **210**(2), 323–329 (2010)
- Hussain, G.; Gao, L.; Hayat, N.; Cui, Z.; Pang, Y.; Dar, N.: Tool and lubrication for negative incremental forming of a commercially pure titanium sheet. *J. Mater. Process. Technol.* **203**(1–3), 193–201 (2008)
- Franzen, V.; Kwiatkowski, L.; Martins, P.; Tekkaya, A.: Single point incremental forming of PVC. *J. Mater. Process. Technol.* **209**(1), 462–469 (2009)
- McAnulty, T.; Jeswiet, J.; Doolan, M.: Formability in single point incremental forming: a comparative analysis of the state of the art. *CIRP J. Manuf. Sci. Technol.* **16**, 43–54 (2017)
- Centeno, G.; Bagudanch, I.; Martínez-Donaire, A.J.; Garcia-Romeu, M.L.; Valleslano, C.: Critical analysis of necking and fracture limit strains and forming forces in single-point incremental forming. *Mater. Des.* **63**, 20–29 (2014)
- Duflou, J.R.; Habraken, A.-M.; Cao, J.; Malhotra, R.; Bambach, M.; Adams, D.; Vanhove, H.; Mohammadi, A.; Jeswiet, J.: Single point incremental forming: state-of-the-art and prospects. *Int. J. Mater. Form.* **11**(6), 743–773 (2018)
- Prashant M, Bhavik P, Vaibhav M, Anukr V.: Single point incremental sheet forming by CNC vertical milling machine. *Imp. J. Interdiscip. Res.* **2**(11) (2016)
- Ziran, X.; Gao, L.; Hussain, G.; Cui, Z.: The performance of flat end and hemispherical end tools in single-point incremental forming. *Int. J. Adv. Manuf. Technol.* **46**(9–12), 1113–1118 (2010)
- Silva, M.; Skjødt, M.; Atkins, A.; Bay, N.; Martins, P.: Single-point incremental forming and formability—failure diagrams. *J. Strain Anal. Eng.* **43**(1), 15–35 (2008)

15. Malwad, D.; Nandedkar, V.: Deformation mechanism analysis of single point incremental sheet metal forming. *Procedia Mater. Sci.* **6**, 1505–1510 (2014)
16. Jagtap, R.; Kashid, S.; Kumar, S.; Hussein, H.: An experimental study on the influence of tool path, tool diameter and pitch in single point incremental forming (SPIF). *Adv. Mater. Process. Technol.* **1**(3–4), 465–473 (2015)
17. Rattanachan, K.; Chungchoo, C.: The effected of single point incremental forming process parameters on the formed part surface roughness. *Adv. Mater. Res.* **979**, 335–338 (2014)
18. Cavaler, L.; Schaeffer, L.; Rocha, A.; Peruch, F.: Surface roughness in the incremental forming of AISI 304L stainless steel sheets. *J. Mechan Eng Phys* **1**(2), 87–98 (2010)
19. Bagudanch, I.; Sabater, M.; Garcia-Romeu, M.L.: Single point versus two point incremental forming of thermoplastic materials. *Adv. Mater. Process. Technol.* **3**(1), 135–144 (2017)
20. Davidson, M.J.; Balasubramanian, K.; Tagore, G.: Surface roughness prediction of flow-formed AA6061 alloy by design of experiments. *J. Mater. Process. Technol.* **202**(1–3), 41–46 (2008)
21. Mulay, A.; Ben, S.; Ismail, S.; Kocanda, A.: Experimental investigations into the effects of SPIF forming conditions on surface roughness and formability by design of experiments. *J. Braz. Soc. Mech. Sci. Eng.* **39**(10), 3997–4010 (2017)
22. Kopac, J.; Kampus, Z.: Incremental sheet metal forming on CNC milling machine-tool. *J. Mater. Process. Technol.* **162**, 622–628 (2005)
23. Cui, Z.; Gao, L.: Studies on hole-flanging process using multistage incremental forming. *CIRP J. Manuf. Sci. Technol.* **2**(2), 124–128 (2010)
24. Lu, B.; Chen, J.; Ou, H.; Cao, J.: Feature-based tool path generation approach for incremental sheet forming process. *J. Mater. Process. Technol.* **213**(7), 1221–1233 (2013)
25. Ambrogio, G.; Filice, L.; Manco, G.: Improving process performance in incremental sheet forming (ISF). *AIP Conf. Proc.* **1315**(1), 613–618 (2011)
26. Cawley, B.; Adams, D.; Jeswiet, J.: Examining tool shapes in single point incremental forming. *Proc NAMRI/SME* **26**, 201–206 (2012)
27. Adams, D.W.: Improvements on Single Point Incremental Forming Through Electrically Assisted Forming, Contact Area Prediction and Tool Development. Queen's University, Canada (2014)
28. Maan, H.Y.: Determining the effect of process parameters on surface roughness in two point incremental sheet metal forming process using the Taguchi method. *Eng. Technol. J.* **33**(7), 1569–1582 (2015)
29. Shah, H.; Chaudhary, S.: Optimization of process parameters for incremental sheet forming process. *Int. J. Technol. Res. Eng.* **3**(7), 2347–4718 (2016)
30. Uttarwar P, Raini S.: Study of effect of process parameters on hardness during incremental sheet metal forming. *Int. J. Eng. Sci.* **3799** (2016)
31. Chinnaiyan, P.; Jeevanantham, A.: Multi-objective optimization of single point incremental sheet forming of AA5052 using Taguchi based grey relational analysis coupled with principal component analysis. *Int. J. Precis. Eng. Manuf.* **15**(11), 2309–2316 (2014)
32. Majagi, S.D.; Chandramohan, G.: Optimization of incremental sheet metal forming parameters by design of experiments. In: *Applied Mechanics and Materials*, pp. 111–116. *Trans Tech Publ* (2014)
33. Majagi, S.D.; Chandramohan, G.; Kumar, M.S.: Effect of incremental forming process parameters on aluminum alloy using experimental studies. In: *Advanced Materials Research*, pp. 633–639. *Trans Tech Publ* (2015)
34. Pandivelan, C.; Jeevanantham, A.: Formability evaluation of AA 6061 alloy sheets on single point incremental forming using CNC vertical milling machine. *J. Mater. Environ. Sci.* **6**(5), 1343–1353p (2015)
35. Mugendiran, V.; Gnanavelbabu, A.; Ramadoss, R.: Parameter optimization for surface roughness and wall thickness on AA5052 Aluminium alloy by incremental forming using response surface methodology. *Procedia Eng.* **97**, 1991–2000 (2014)
36. Suriyaprakan P.: Single Point Incremental Forming and Multi-Stage Incremental Forming on Aluminium Alloy 1050. *Thammasat University* (2013)
37. Chang, Z.; Chen, J.: Mechanism of the twisting in incremental sheet forming process. *J. Mater. Process. Technol.* **276**, 116396 (2020)
38. Echrif, S.B.; Hrairi, M.: Significant parameters for the surface roughness in incremental forming process. *Mater. Manuf. Process.* **29**(6), 697–703 (2014)

Springer Nature or its licensor holds exclusive rights to this article under a publishing agreement with the author(s) or other rightsholder(s); author self-archiving of the accepted manuscript version of this article is solely governed by the terms of such publishing agreement and applicable law.